AD-750 413

New Techniques for the Syntheis of Metals and Alloys

California University

prepared for
Advanced Research Projects Agency

SEPTEMBER 1972

Distributed By:

NTIS

National Technical Information Service
U. S. DEPARTMENT OF COMMERCE
5285 Port Royal Road, Springfield Va. 22151

BEST
AVAILABLE COPY

AD 750413

DDC
RECEIVED
OCT 31 1972
B

SEMI-ANNUAL TECHNICAL REPORT NO. 4

UCLA-ENG-7288
SEPTEMBER 1972

EW TECHNIQUES FOR THE SYNTHESIS F METALS AND ALLOYS

R.F. BUNSHAH

Reproduced by
NATIONAL TECHNICAL
INFORMATION SERVICE
U S Department of Commerce
Springfield VA 22151

This research was sponsored by the Advanced Research Projects Agency of the Department of Defense under Contract No. DAHC 15-70-C-16

DISTRIBUTION STATEMENT A
Approved for public release;
Distribution Unlimited

Security Classification

DOCUMENT CONTROL DATA - R & D

(Security classification of title, body of abstract and indexing annotation must be entered when the overall report is classified)

1. ORIGINATING ACTIVITY *(Corporate author)*

School of Engineering & Applied Science
University of California at Los Angeles
Los Angeles, California 90024

2a. REPORT SECURITY CLASSIFICATION

Unclassified

2b. GROUP

3. REPORT TITLE

I. NEW METHODS OF SYNTHESIS OF MATERIALS

4. DESCRIPTIVE NOTES *(Type of report and inclusive dates)*

Semi-Annual Technical Report

5. AUTHOR(S) *(First name, middle initial, last name)*

I. R.F. Bunshah

6. REPORT DATE

September 1972

7a. TOTAL NO. OF PAGES

39

7b. NO. OF REFS

27

8a. CONTRACT OR GRANT NO.

AO #1643

b. PROJECT NO.

c.

d.

9a. ORIGINATOR'S REPORT NUMBER(S)

UCLA-ENG-7288

9b. OTHER REPORT NO(S) *(Any other numbers that may be assigned this report)*

10. DISTRIBUTION STATEMENT

Distribution of this document is unlimited

11. SUPPLEMENTARY NOTES

12. SPONSORING MILITARY ACTIVITY

Advanced Research Projects Agency
Department of Defense

13. ABSTRACT

Two major areas of effort are encompassed:

I. New Techniques for the Synthesis of Metals and Alloys

The high rate physical vapor deposition (HRPVD) process is to be used for the following:

1. Preparation and characterization of Ni and Ni-20Cr alloy sheet
2. Synthesis of compounds Y_2O_3, TiC, Si_3N_4 by reactive evaporation and their characterization.
3. Dispersion strengthened alloys. Ni-20Cr-Y_2O_3, Ni-20Cr-TiC and Ti-Y_2O_3.

This report describes:

1. The evaporation of a Ni-20Cr alloy from a single rod fed electron beam source.
2. The effect of substrate temperature on the structure and properties of TiC prepared by Activated Reactive Evaporation.

14. KEY WORDS	LINK A		LINK B		LINK C	
	ROLE	WT	ROLE	WT	ROLE	WT
Activated reactive evaporation						
Carbides						
Condensation						
Deposit						
Evaporation						
Evaporation apparatus						
Hafnium carbide						
High Rate Physical Vapor Deposition Process						
Laser						
Lattice parameter						
Microhardness						
Nichrome						
Nickel						
Nitrides						
Oxidation						
Oxides						
Pool height monitor						
Pressure barrier						
Reactive evaporation						
Refractory carbides						
Silicon nitride-Si_3N_4						
Substrate						
Synthesis of Materials						
Thickness distribution						
Titanium carbide						
Yttria-Y_2O_3						
Yttrium						

ib

UCLA-ENG-7288
September 1972

SEMI-ANNUAL TECHNICAL REPORT NO. 4

I. New Techniques for the Synthesis of Metals and Alloys
(Principal Investigator - Professor R.F. Bunshah)

Sponsor: The Advanced Research Projects Agency

Grant No.: DAHC 15-70-G-15

ARPA Order No.: AO 1643

Effective Date: July 1, 1970

Contract Expiration Date: June 30, 1973

Amount of Contract: $298.398

Classification: Un-classified

Materials Department
School of Engineering and Applied Science
University of California
Los Angeles, California

ABSTRACT

I. New Techniques for the Synthesis of Metals and Alloys

The high rate physical vapor deposition (HRPVD) process is to be used for the following:

1. Preparation and characterization of Ni and Ni-20Cr alloy sheet.
2. Synthesis of compounds Y_2O_3, TiC, Si_3N_4 by reactive evaporation and their characterization.
3. Dispersion strengthened alloys, Ni-20Cr-Y_2O_3, Ni-20Cr-TiC and Ti-Y_2O_3.

This report describes:

(1) The evaporation of a Ni-20Cr alloy from a single rod fed electron beam source.

(2) The effect of substrate temperature on the structure and properties of TiC prepared by Activated Reactive Evaporation.

TABLE OF CONTENTS

PART I

NEW TECHNIQUES FOR THE SYNTHESIS OF METALS AND ALLOYS (TASKS I, II, AND III)

R. F. Bunshah

INTRODUCTION

This report describes research activities on ARPA Grant No. AO 1643. The scope of the work is divided into two major areas of effort and further subdivided into four tasks as shown below

1. New Techniques for the Synthesis of Metals and Alloys - Tasks I, II, and III. (Professor R.F. Bunshah - Principal Investigator)
2. The Properties of Rare Earth Metals and Alloys - Task IV (Professor D. L. Douglass - Principal Investigator)

In the following, progress on Tasks I, II and III is reported. Progress on Task IV is being issued as a separate report.

I. Background

High rate physical vapor deposition (HRPVD) techniques[1-8] are to be used to prepare metallic alloys, ceramics, and metal-ceramic mixtures (dispersion strengthened alloys). The method consists of evaporation of metals, alloys and ceramics contained in water cooled crucibles using high power electron beams. The process is carried out in a high vacuum environment. The use of high power electron beams makes it possible to produce very high evaporation rates. The vapors are collected on heated metallic substrates to produce full density deposits at high deposition rates.

There are three tasks in this section:

Task 1: The preapration and characterization of nickel and Ni-20Cr alloy sheet by the high rate physical vapor deposition process.

Task II: Synthesis and characterization of compounds by Reactive Evaporation. The compounds to be prepared are Y_2O_3, TiC and Si_3N_4.

Task III: Dispersion strengthened alloys produced by HRPVD Process, and their characterization. The specific alloys to be studied are:

A. Ni-20Cr-Y_2O_3 B. Ni-20Cr-TiC C. Ti-Y_2O_3

Single source and two source evaporation methods will be used to produce these alloys.

The HRPVD process has several attractive features:

A. Simple, full density shapes (sheet, foil, tubing) can be produced at high deposition rates, 0.001" per minute thickness increment thus making it an economically viable process.

B. Metals and alloys of high purity can be produced.

C. Very fine grain sizes (1μ grain diameter or smaller) can be produced by controlling substrate temperature. Grain size refinement is

produced by lowering the condensation temperature.

D. An alloy deposit may be produced from a single rod fed source. This occurs because the molten pool at the top of the rod is about 1/4" deep only. The vapor composition is the same as that of the solid rod being fed into the molten pool. At equilibrium, the composition of the molten pool differs from that of the vapor or the solid feed. It is richer in those components having a low vapor pressure. The composition of the vapor is the product of the vapor pressure times the mole fraction of the component. For example, a Ti-6Al-4V alloy deposit where the differences in vapor pressure of Al and V are a factor of 5,000 at 1600°C can be produced by evaporation from a single source. The feed-rod is Ti-6Al-4V and the molten pool is much richer in V than in Al.

E. Two or more sources can be used to simultaneously deposit on the same substrate thus conferring the ability to produce complex alloys. For example, an alloy with a 2 or 3 component solid solution matrix may be evaporated from one source and another metal or ceramic for the dispersed phase from another source. The dispersion size and spacing should be very fine since the deposition is occurring from the vapor phase.

The unique feature of this process is that all of the above benefits can be obtained <u>simultaneously</u>.

It should be noted that the condensation temperature is a very important process variable. Bunshah and Juntz[8] found that for titanium, as the deposition temperature is lowered the grain size of the fully dense deposit becomes finer. At very low temperatures (~25% of the melting point) the deposit has less than full density.

Since a fine grain sized microstructure represents an optimum condition of strength and toughness in a material, the importance of control over the deposition temperature becomes obvious.

II. Scope of work and progress in reporting period (February 1, 1972 - August 31, 1972)

The main tasks on this contract are the preparation and testing of the various alloys, ceramics and dispersion strengthened alloys as outlined in Section I above. Very essential to the preparation of suitable test specimens are two other factors:

A. Design of the apparatus for high rate physical vapor deposition.

B. Theoretical calculation of the thickness distribution and temperature distribution of the deposited material which is in this case in the form of a sheet.

Both of these tasks are essential preliminaries to the main scope of work. They were completed and described in semi-annual technical report No. 1.[9]

Two papers based on item B above have been published.[10,11]

A new process for the synthesis and high rate deposition of compounds was developed.[12] The process is called Activated Reactive Evaporation and two papers[13,14] have been presented and accepted for publication. During this reporting period, further work was done relating the synthesis, stoichiometry and microstructure (internal and external) for TiC, ZrC and (Hf-3Zr)C. It is described in detail in Supplement I of this report.

In addition, considerable development work was done on two important experimental equipment items, i.e., the Laser Pool Height Monitor and the Pressure Barrier. They are described below.

The present system is used for a great number of diverse experiments, many of which do not require a pressure barrier. Therefore, the design of the pressure barrier must allow for easy removal, total or partial. The surface of the barrier which covers the filament of the electron gun must be able to withstand a large radiant heat flux. It must be possible to use the pressure barrier with different electron guns, all of which do not have the same constructural geometry.

The pressure barrier shown in Fig. 1, meets all the design criteria specified above. The plate is 1/8" thick stainless steel and is held in position by only four bolts. In addition to the closeable port which is shown, there are two other large ports which have removable covers. In the center of the stainless steel plate is an interchangeable copper plate. This copper plate is held to the upper stainless steel plate by four bolts, with an o-ring between the two plates, and is water cooled to dissipate the large radiant heat flux of the filament and molten pool of metal. When a different electron gun is to be used, a different copper plate is also used. This provides a high degree of refinement with respect to heat transfer considerations.

A lower support ring is held flush to the base plate with four clamps. This ring and the plate furnish the support for the removeable walls. These walls are made of 0.005 in. thick stainless steel sheet and are in two sections. Short lengths of drill rod are spot welded to the stainless steel sheet periodically along the length and in the direction perpendicular to the plane of the plate. The addition of the drill rod has a negligible effect on the weight of the walls, and greatly increases their rigidity in the critical direction. The walls are made in two sections for ease in removal. Gross vacuum leaks at the joints between the two sections are eliminated by double interlocking flaps. When mounted, the two sections are held together with spring-loaded hooks.

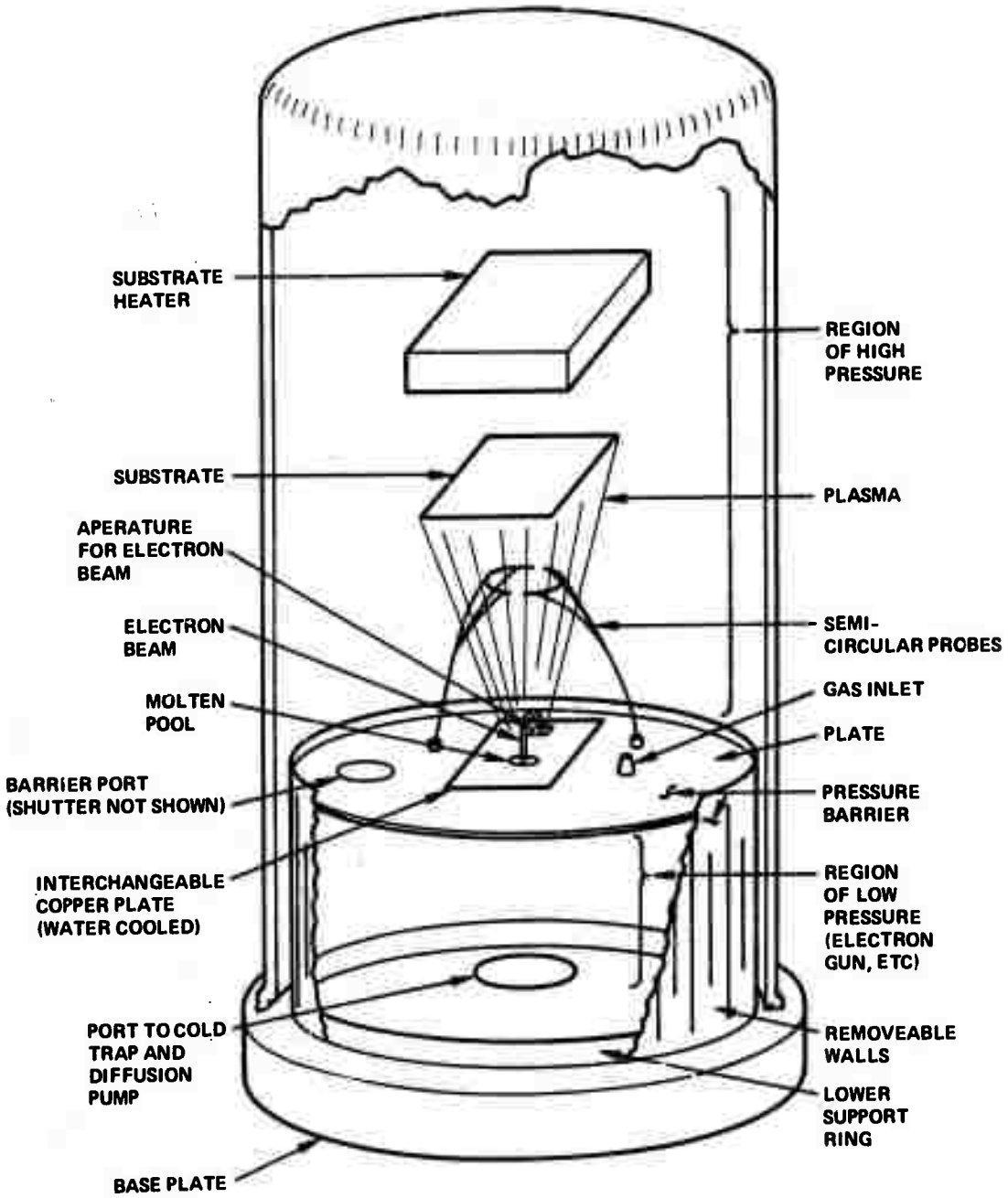

Figure 1. Section of Bell Jar — Revealing Essential System Features

The laudable features of the design are its simplicity, inexpensive construction, adaptibility to various system parameter changes, and ease of usage.

If an experiment is to be performed which does not require a pressure barrier, the removable walls are removed and the two extra ports in the plate are uncovered, i.e., the plate and lower support ring remain intact.

At the present time, the pressure barrier has been tested successfully. Without any gaskets between the plate, lower support ring, base plate, and the removable walls, a pressure differential of two orders of magnitude can be maintained. The ultimate limitation to the value of the differential pressure is the aperture in the plate for the passage of the electron beam from the underside to the molten pool on the upper side. The ultimate rate of deposition has not yet been determined, but already TiC films have been deposited at the rate of 0.00068 in./min. at a partial pressure of C_2H_2 of 10μ. This is slightly more than twice the rate attained without the pressure barrier. It is anticipated that further experiments will indicate that the allowable rate is much greater.

B. Pool Height Monitor

In a rod fed evaporation source, there is a molten pool about 1/8 to 1/4" deep on top of the solid rod from which the material evaporates. In practice, the molten pool can be run high (i.e., a meniscus above the level of the top of the crucible) or low (i.e., at or below the level of the top of the crucible). The heat loss by radiation from the molten pool under these two conditions is significantly different and will change the depth and consequently the volume of the molten pool as well as the shape of the meniscus.

Several considerations arise which are as follows:

1. In alloy evaporation, discussed previously,[12] variation in pool volume produces a marked change in the composition of the vapor and hence of the deposit. This is a very important consideration.

2. Change in meniscus shape (concave or convex) and radius of curvature will produce a change in evaporation rate and distribution on the substrate.

It was decided therefore to build a pool height monitor. Several options are possible of which two were considered seriously.

1. The rate of change of weight of the billet could be monitored. However, it is a difficult proposition.

2. An intense light source could be directed across the surface of the molten pool and detected on the opposite side. If the billet is raised too high, the beam is attenuated. The billet movement may be either stopped or reversed at this point, with the choice being made by the degree of response of the mechanical drive system. The system layout is shown in Fig. 2. The electronics for the controlling portion of the monitor are shown in Fig. 3. As designed, the circuit reverses the direction of billet travel when it gets too high. The reason for this is that the large inertia associated with the mechanical system shown in Fig. 1. will cause overshoot. Since the laser beam is well defined, the billet will simply oscillate within a narrow band. Tuning the circuit to eliminate the radiated light from the molten pool is done by changing the bias on the second operational amplifier. The biasing was put on the second op amp to make the circuit element values less critical. The entire circuit is placed in a grounded aluminum box to minimize the effects of thermal gradients and environmental noise.

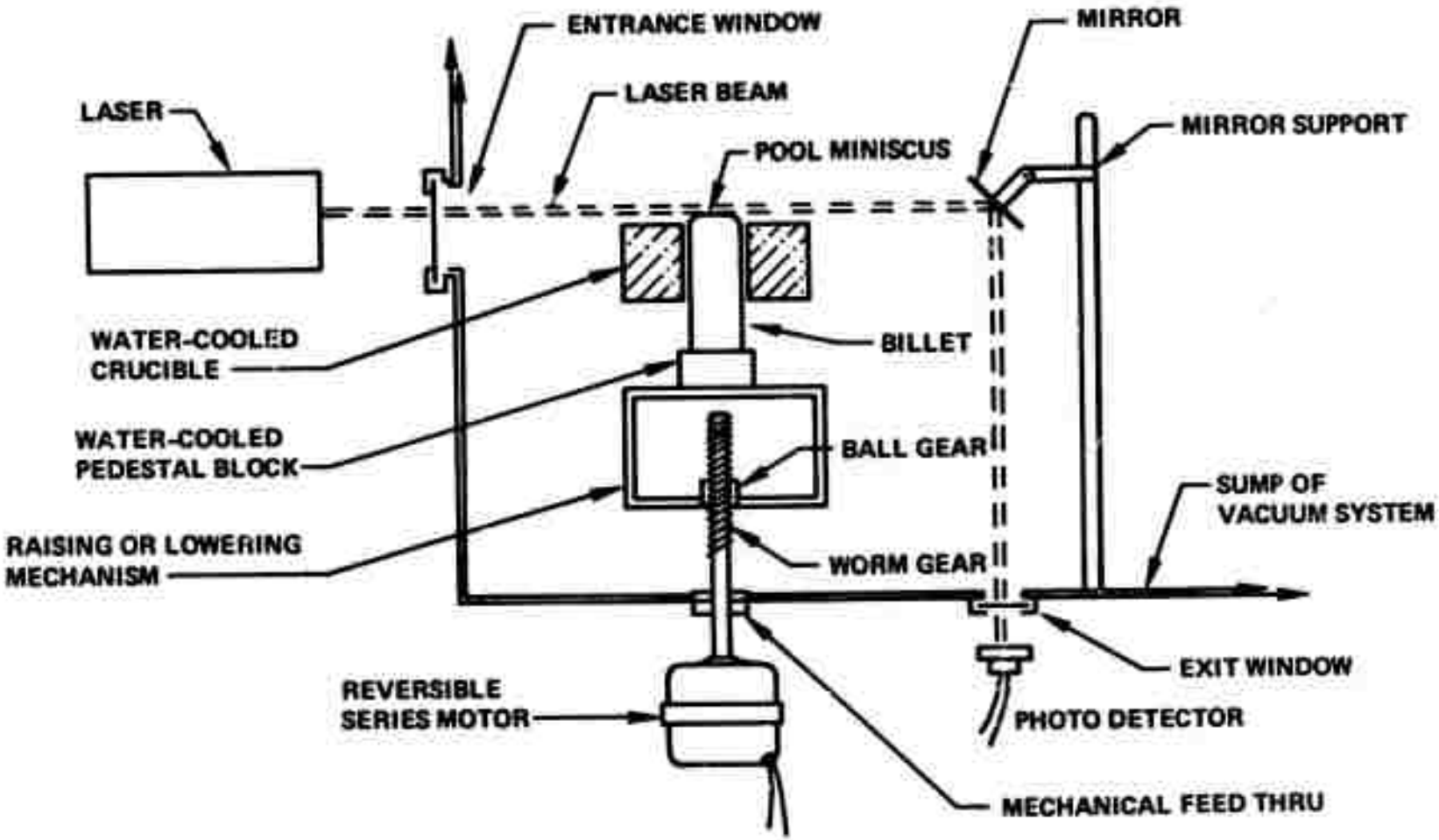

Figure 2. System Layout for Laser Pool-Height Monitor

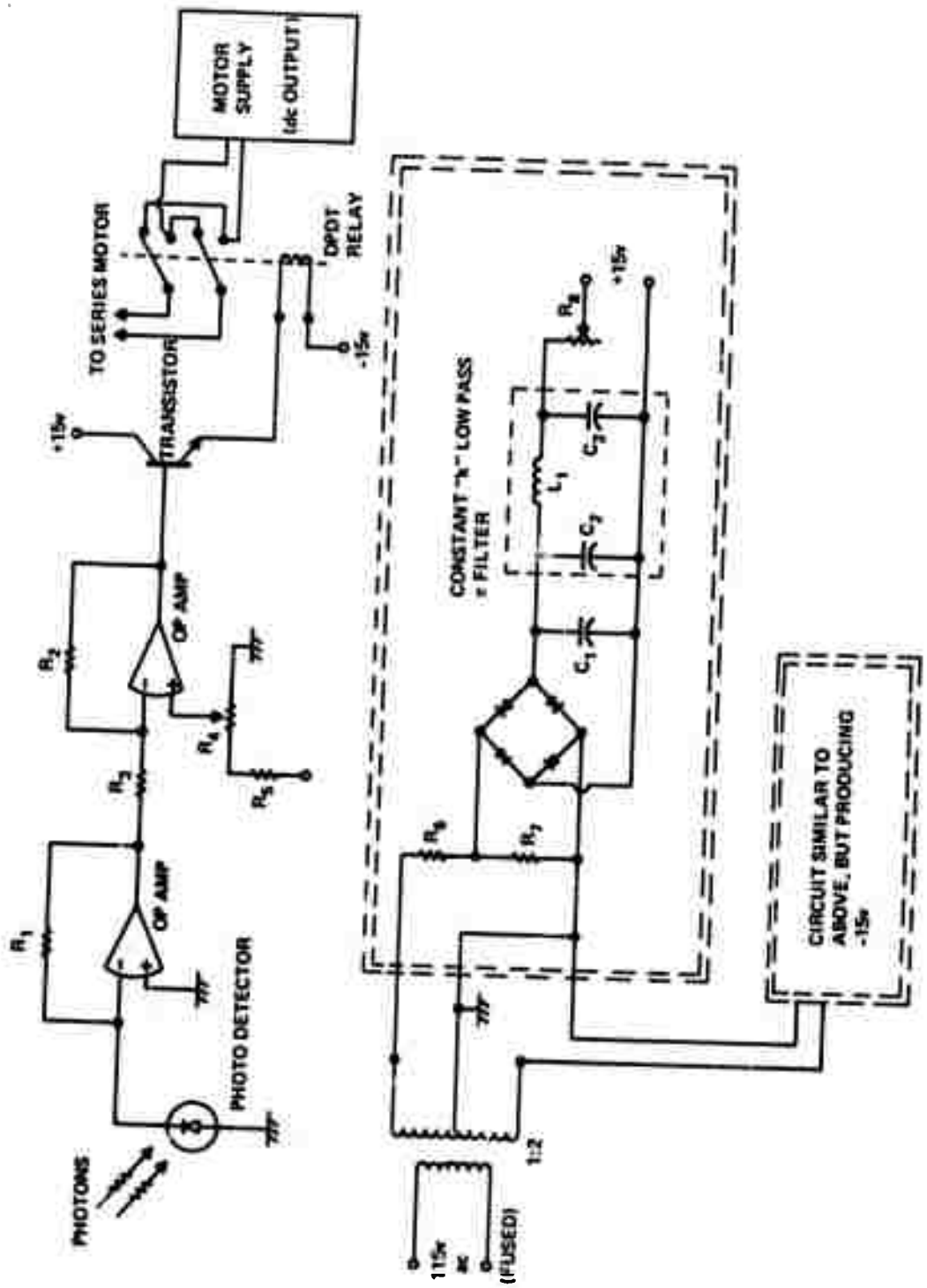

Figure 3. Schematic of Controller for Laser Foil-Height Monitor

III. Future Work

In the next half-year period, the following work is scoped.

A. Continuation of the work on deposition of Ni and Ni-20Cr alloy sheets and a study of their structure and properties.

B. Continuation of the work on the synthesis and testing of Y_2O_3, TiC, and Si_3N_4 by reactive evaporation and activated reactive evaporation.

C. Initiation of the work on production of Ni-20Cr alloys containing dispersed phases by HRPVD processes from two evaporation sources.

IV. Personnel

The following personnel have been working on this project in this reporting period.

Principal Investigator - Professor R. F. Bunshah

Post Doctoral Fellows: Dr. A. C. Raghuram and Dr. H. A. Beals

Graduate Students: Mr. Rao Nimmagadda and Mr. Neil Kane

Technician: Mr. Fred Weiler

In addition, Professor C.N.J. Wagner of the Materials Department contributed his time and guidance for the analysis of the internal structure of the carbide deposits.

REFERENCES

1. Bunshah, R. F., "Superpurification of Metals by Vacuum Distillation: A Theoretical Study," Trans. Vac. Met. Conf., 1963, AVS, 121.

2. Bunshah, R. F., and Juntz, R. S., "Purification of Beryllium by Crucible Free Melting and Distillation Process" in Beryllium Technology, Gordon and Breach, 1964, 1.

3. Bunshah, R. F., "Impurity Removal by Distillation of Beryllium from the Solid State," Proceedings, Int'l. Conf. on Beryllium, Grenoble, France, 1965, Presses Universitaries de France, 108 Blvd. St. Germain, Paris, 6, 63.

4. Bunshah, R. F., and Juntz, R. S., "The Purification of Beryllium by Vacuum Melting followed by Vacuum Distillation in an Electron Beam Furnace with Simultaneous deposition of Sheet," Trans. Vac. Met. Conf., 1966, AVS, 209.

5. Bunshah, R. F., "The Effect of Purification on Some Mechanical Properties of Beryllium," Metals Engineering Quarterly, Nov. 1964, 8.

6. Bunshah, R. F., and Juntz, R. S., "Electron Beam Distillation Furnace for Reactive Metals: Design Considerations and Operating Experience," Trans. Vac. Met. Conf., 1965, AVS, 200.

7. Bunshah, R. F. and Juntz, R. S., "Design Considerations for the Production of Massive Deposits of Alloys by Evaporation from Multiple Electron Beam Heated Sources," Trans. Vac. Met. Conf., 1967, AVS, 799.

8. Bunshah, R. F., and Juntz, R. S., "Influence of Condensation Temperature on Microstructure and Mechanical Properties of Titanium Sheet," to be published.

9. Bunshah, R.F., and Douglass, D. L., Technical Report - UCLA-Eng-7112, March, 1971.

10. Nimmagadda, R., and Bunshah, R.F., J. Vac. Sci. and Tech., December 1971.

11. Chow, R., and Bunshah, R.F. to be published in J. Vac. Sci. and Tech., December 1971.

12. Bunshah, R.F., and Douglass D.L., Technical Report-UCLA-Eng-7227 April 1972.

13. Bunshah, R.F. and Raghuram, A.C., "The Activated Reactive Evaporation Process," to be published, Jul. Vac. Sci. Tech. Nov/Dec. 1972.

14. Raghuram, A.C. and Bunshah, R.F., "The Influence of Substrate Temperature on the Structure of Titanium Carbide produced by Activated Reactive Evaporation," Jul. Vac. Sci. Tech. Nov/Dec. 1972.

Supplement I

Structure and Mircohardness Relationships in Ti, Zr and Hf-3Zr Carbide Deposits Synthesized by Actived Reactive Evaporation

I. Introduction and Objective

The carbides of the group IV elements Ti, Zr and Hf are technologically important materials because of the high hardness they exhibit.[1] For example TiC exhibits a Knoop hardness of 3100 kg/mm^2 for a 50 gram load, and is the third hardest material known after diamond (7,000 kg/mm^2) and cubic boron nitride (4,500 kg/mm^2). The properties of these ceramic materials are strongly dependent on imperfection content, particularly impurity content, and on stoichiometry, i.e., carbon to metal ratio over the wide solubility range exhibited by these carbides.

Recently, a technique called "Activated Reactive Evaporation"[2,3] has been developed for the high rate deposition of compounds, i.e., about 125,000Å per minute as compared to 1,000Å per minute for sputtering. In this investigation, thick deposits, about 100 μm thickness, were produced on metallic substrates using this technique. They were characterized by microstructure lattice parameter and microhardness measurements.

II. The Activated Reactive Evaporation Process

Since the "Activated Reactive Evaporation" (ARE) technique[2.3] is a new process which has not yet been published, it is briefly described.

A reaction between metal vapor atoms and gas molecules results in the formation and deposition of a compound. To this extent, it is similar to the "Reactive Evaporation" process.[4] The ARE process has been developed

to produce a high deposition rate of a compound. Therefore, the metal vapor density and the gas molecule density in the reaction zone must be sufficiently high to provide a high collision frequency between the reacting species. In our case, see Fig. 1, the high vapor density is provided by an electron beam heated pool, of molten metal or alloy contained in a water-cooled copper crucible. The reactive gas is introduced at a high partial pressure ($\sim 10^{-4}$ torr) in the chamber. Since the mean free path decreases with increasing partial pressure, the reaction zone in our case is located in the space above the metal vapor source and below the substrate. At lower partial pressures, as in reactive evaporation, the mean free path is larger than the source-to-substrate distance and collision between reacting species occurs only on the substrate.

A high collision frequency does not insure a high reaction rate between the components. For many cases, e.g. $2Ti+C_2H_2 \not\rightarrow 2TiC+H_2$, the reaction has to be stimulated by activating one or both of the reactants. In the ARE process, this is done by placing an electrode at a + positive potential ($\sim$100 to 250 V) above the pool. This draws the primary and secondary electrons above the pool into the reaction zone thus ionizing and activating the reactants. For high rate deposition of a compound, it is essential that "activation" of the reactants occurs in the reaction zone. Variations of the "Reactive Evaporation" process proposed in the literature have activated the reacting gas by a glow discharge or microwave discharge outside the reaction zone.[5] This would not be sufficient for a high rate of deposition of the compound since activated gases become deactivated on collision with other gas molecules or surfaces in the gas path e.g. the tube through which the gas flows.

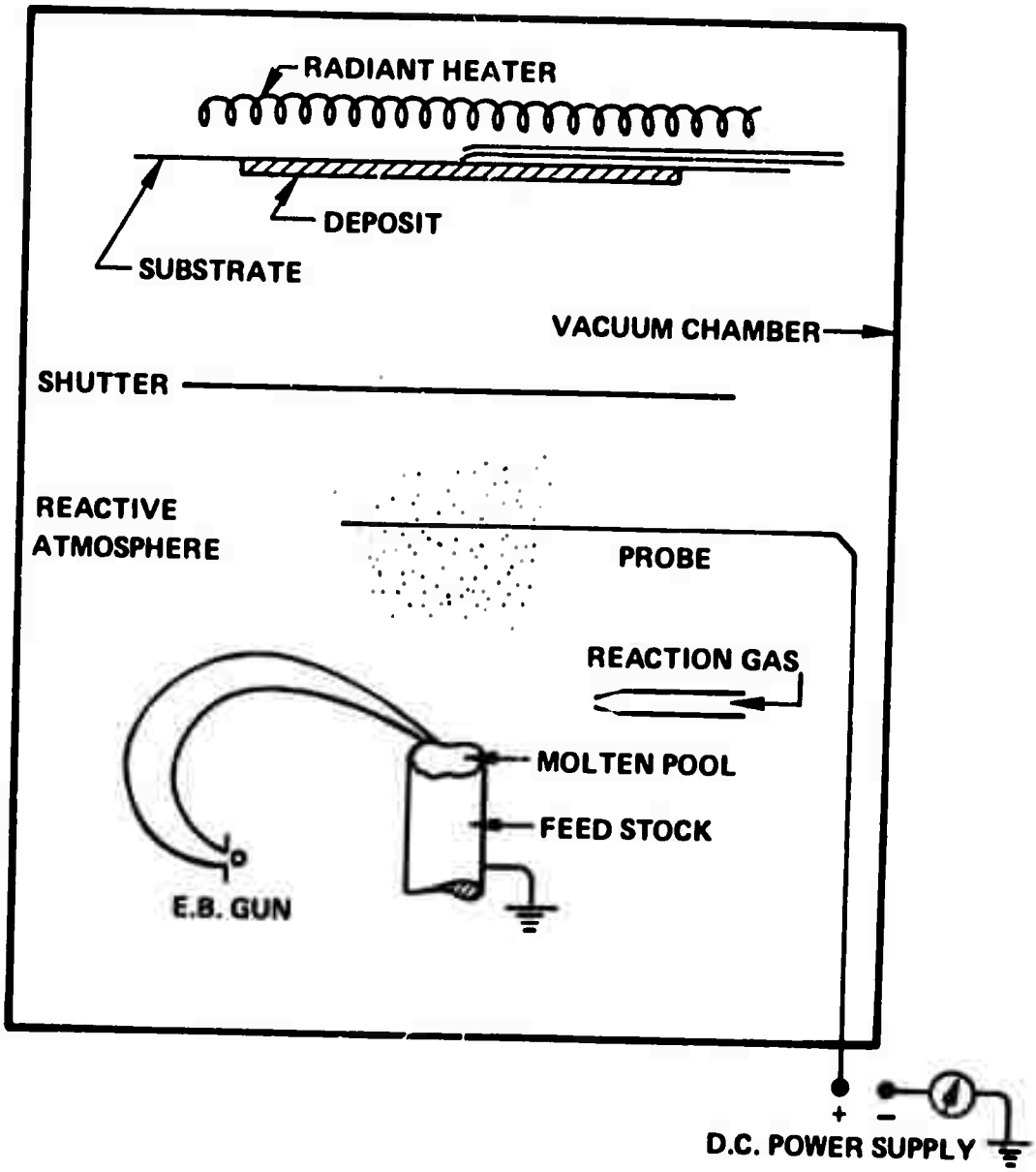

Figure 1. Schematic of the Experimental Arrangement for the Activated Reactive Evaporation Process.

This process is a good example of reaction kinetics. The rate governing step can be either the supply of the reactants to the reaction interface, the collision frequency between the reactants, the probability of reaction between the colliding species or the rate of removal of the reactants from the reaction interface. For the synthesis of TiC, no compound formation occurs in the absence of the activation step.[3] With activation, compound formation occurs readily and the stoichiometry of the carbide and/or the presence of excess titanium in the deposit can be varied by changing the supply of either reactant as will be illustrated later.

III. Experimental Details

A. Materials, Apparatus and Procedure

The materials used for evaporation were arc melted Ti, Zr and Hf-3Zr alloy rods 1" in diameter by 5" long. The composition of the materials is given in Table I under the column evaporant. Also given in Table I are the analysis of metallic deposits from the Ti[6] and the Hf-3Zr alloy[7] carried out previously in other investigations. This gives an idea of the impurity contamination of the deposit which can be attributable to the source. Acetylene is used as the reacting gas. It contains less than 0.4 volume pct. impurities, which are principally CH_4, N_2 and H_2.

The metals are evaporated from a rod-fed electron beam source contained in a vacuum chamber, a 24" diameter stainless steel bell jar 30" high, see Fig. 1. The base pressure of the system is 2×10^{-7} torr. The reacting gas is supplied through a regulated opening to tubes located in the vicinity of the reaction zone. The probe activating the reaction is located in the reaction zone and is biased to a positive voltage between 80 and 250 VDC.

Table I

Chemical Composition of Evaporant Rods in ppm wt.pct.

	Ti		Zr	Hf-3Zr	
	Evaporant	Distillate	Evaporant	Evaporant	Distillate
O_2	0.2	0.035	0.019	.005	.005
N_2	0.05	0.015	0.0006	.0005	.0005
C	0.015	0.007	0.003	.001	.001
H_2	0.25	0.0001	0.0046	-	-
Fe	0.20	0.1200	0.0075	.005	.005
Mg	0.12	0.001	0.0008	.001	.001
Si	0.04	0.0005	0.003	-	-
M	0.02	0.002	0.0006	-	-
Co	0.02	0.001	-	-	-
Al			0.0020	-	-
Ca			0.0030	-	-
Cr			0.0030	.001	.001
Cu			0.0025	.002	.002
Hf			0.0320	Bal.	Bal.
Ni			0.003	.001	.001
Zr			Bal.	3.1	3.1
Ti	Bal.	Bal.			

The deposits are collected on substrates in the form of sheet 8 in x 8 in in size and 125 μm thick located 6" from the pool. The substrates are heated to a temperature of 500°C. The temperature is monitored by a chormel-alumel thermocouple spot welded to the back of the substrate. For TiC deposition, the substrate was stainless steel. For ZrC and (Hf-3Zr)C, the substrate was zirconium sheet.

The experimental procedure is as follows. With the shutter closed, the system is pumped down to its base pressure and then the pressure is raised to 5.10^{-4} torr by bleeding in C_2H_2. The gas supply is closed and the system pumped down again. This procedure is repeated three times. The substrate is then heated to the desired temperature. Next the electron beam is activated, a molten pool established and the beam current is adjusted to provide the desired evaporation rate. The desired gas pressure is established in the system. The potential is next applied to the probe and a stable discharge is observed as a glow in the reaction zone and a probe current of about 200 ma. The shutter is then opened and the deposit collected on the substrate.

Microhardness measurements were made on a Kentron microhardness tester using a Knoop indentor and a load of 50 grams. The results of several indentations are averaged. The depth of indentation was calculated to be about 1.5 μm whereas the thickness of the deposit is 100 μm. Hence the measurements reflect the true hardness of the deposit.

The external microstructure was observed by optical microscopy and photo-emission electron microscopy (courtesy of Balzers. Lichtenstein).

The internal microstructure was deduced from X-ray diffraction analysis.[8] The positions of the maxima of the powder pattern peaks yield the lattice parameter a_o, residual stresses σ, and faulting probability α, whereas the profiles enable us to determine the particle size D and internal strains ε.

The powder pattern peaks of all carbide deposits were scanned at a quarter degree per minute on a Norelco diffractometer using filtered Cu Kα radiation. All peaks, which were Fourier analyzed; i.e., the (111) (222) and (200) (400) pairs, were resolved into their α_1 and α_2 components by means of the Riechinger correction.[8] Some high angle reflections were also Riechinger corrected, and it was found that the maxima of the Kα peak and the uncorrected $K\bar{\alpha}$ peak yielded identical lattice parameters when using $\lambda K\alpha_1 = 1.5418\text{Å}$ and $\lambda K\bar{\alpha} = 1.5405\text{Å}$, respectively. Therefore, most lattice parameters a_{hkl} were determined from the peak maximum of the Kα doublet, and plotted as a function of $\cos\theta \cot\theta$. A Si powder specimen was used to calibrate the experimental set-up, and a_o was found to be 5.4302 ± 0.0002A.

In order to quantitatively examine the broadening produced by the internal microstructure of the carbide deposits, the profiles of the (111), (222), (200) and (400) reflections were represented as a Fourier series in reciprocal space.

The $K\alpha_1$ profile of a powder pattern pattern peak $P(2\theta)$ is given by a cosine Fourier series:

$$P(2\theta) = K \sum_{n=-\infty}^{+\infty} A(L) \cos 2\pi L (S-S_o)$$

where K is a proportionality constant, $L = nd_{hkl}$, $S = 2\sin\theta/\lambda$, and $S_o = 2\sin\theta_o/\lambda = 1/d_{hkl}$, d_{hkl} being the interplanar spacing between (hkl) planes.

The Fourier coefficients A(L) can be expressed as

$$A(L) = A^P(L) \cdot A^D(L) . \qquad (1)$$

$A^P(L)$ are the particle size coefficients which are independent of the order of reflection, and $A^D(L)$ are the strain coefficients, which can be approximated for small values of the strains $\langle\varepsilon\rangle$ as

$$A^D(L) = 1 - 2\pi^2 L^2 [\langle\varepsilon^2\rangle - \langle\varepsilon\rangle^2] S_o^2 , \qquad (2)$$

where $\langle\varepsilon\rangle$ is the mean strain, and $\langle\varepsilon^2\rangle$ is the mean square strain in the coherently diffraction domains (grains, subgrains or particles) of average size $\langle D\rangle$, which can be obtained from the initial slope of the $A^P(L)$ vs L curves, i.e.,

$$(dA^P(L)/dL)_{L\to 0} = - 1/\langle D\rangle. \qquad (3)$$

In order to separate particle size and strain, one employs the Warren-Averbach method which follows from equations (1) and (2), i.e.,

$$\ell n\, A(L) = \ell n\, A^P(L) - 2\pi^2 L^2 [\langle\varepsilon^2\rangle - \langle\varepsilon\rangle^2] S_o^2 \qquad (4)$$

When plotting $\ell n\, A(L)$ as a function of $S_o^2 = 1/d_{hkl}^2 = (h^2 + k^2 + l^2)/a_o^2$ for different values of L, the intercept with the ordinate will yield $\ell n\, A^P(L)$ and the slope will be proportional to $[\langle\varepsilon^2\rangle - \langle\varepsilon\rangle^2]$.

All computations including Rachinger correction, the Stokes correction for instrumental broadening, Fourier analysis and strain-particle size separation, were carried out on an IBM 360-91 computer using a FORTRAN IV Program.

IV. Results and Discussion

In the ARE process, the acts of compound synthesis and deposit growth are separate since the former occurs in the vapor phase and the latter on the substrate. This is a very important advantage since it permits one to vary the substrate temperature at will and change the microstructure and mechanical properties of the deposit.

As reported elsewhere,[9] the morphology and microhardness of TiC deposits can be drastically changed by varying the substrate temperature. A change in substrate temperature from 500 to 1100°C changes the morphology

from tapered crystallite growth to columnar grains and the microhardness from 3000 to 5000 kg/mm^2 for a 50 gram load.

All the carbides considered here have a f.c.c. B_1 crystal structure and exhibit a wide range of solubility, particularly TiC. Their properties are strongly dependent on stoichiometry (i.e. cation and anion deficiencies) and impurity content.

The data on each of the carbides will be considered separately.

A. Titanium Carbide

The structure of the deposit is too fine to be resolved by optical microscopy. Fig. 2 shows a cross section of the deposit using a photo-emission electron microscope. The specimen had been prepared by diamond grinding and polishing. The resolution of the microscope is about 0.1 μm. The grain size is of the same order as it is barely resolved. Fig. 3 is a photomicrograph showing the substrate and the deposit with a marked diffusion zone about 2μm deep between the two. This produces a very strong bond between the substrate and the deposit. The specimen can be completely bent on itself with the carbide on the tension side without any parting of the deposit or even chipping of the deposit. The carbide cracks internally as evidenced by audible clicks during bending.

Tables II and III show the lattice parameter a_o and the microhardness data as a function of the synthesis parameters for TiC. The lattice parameter a_o was obtained by a least square extrapolation of a_{hkl} to $\cos\theta \cot\theta = 0$ as shown in Fig. 4.

The carbon-to-metal (C/M) ratio is given as a range and was obtained by referring the measured lattice parameter to the data on lattice parameter vs. C/M ratio given by Storms[1] and reproduced in Fig. 5 a,b,c. The depression following the maximum is attributed by Storms to oxygen contamination.

Figure 2. Cross-Section of TiC Deposit at 500°C Substrate Temperature. Grain Size 0.1μ. Magnification 4000 X (courtesy Balzers AG, Liechtenstein).

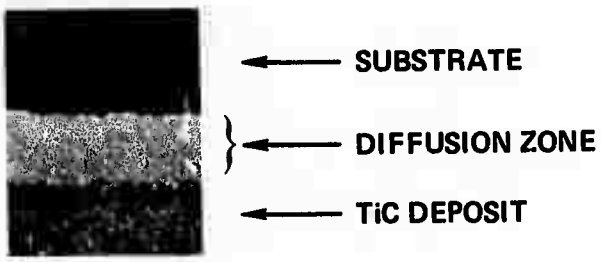

Figure 3. Photomicrograph Illustrating the Bond Between the Substrate and Deposit. Note the Diffusion Zone. Magnification 4000 X.

Table II

Variation of Lattice Parameter, $[\frac{C}{M}]$ Ratio and Microhardness with Pressure of Reactive Gas for TiC

Sample	$P_{C_2H_2}$ torr	Rate of Evaporation g/min	Rate of Deposition m/min	Lattice Parameter Å	Carbon to Metal Ratio $[\frac{C}{M}]$	Microhardness (50 g load) DPHN kg/mm^2	Particle Size <D>in A	Strain $[\langle\varepsilon_L^2\rangle - \langle\varepsilon_L\rangle^2]^{1/2}$ in%
	1×10^{-4}	0.67	4	-	Ti + TiC	-		
34-4	3×10^{-4}	0.67	4	4.308±.003	0.5-0.6	2,000	180	0.33
35-3	4×10^{-4}	0.67	4	4.317±.002	0.62-0.64	2,550	160	0.24
	5×10^{-4}	0.67	4	4.322±.003	0.64-0.70	2,775	-	-
34-6	$7\text{-}8 \times 10^{-4}$	0.67	4	4.329±.001	0.73-0.96	2,670	200	0.21

Variation of Littice Parameter, $[\frac{C}{M}]$ Ratio and Microhardness with Rate of Evaporation of Ti for TiC

Sample No.	$P_{C_2H_2}$ torr	Rate of Evaporation g/min	Rate of Deposition μm/min	Lattice Parameter Å	Carbon to Metal Ratio $\frac{C}{[M]}$	Microhardness 50 g load DPHN /mm^2	Particle Size <D>in A	Strain $[\langle\varepsilon_{L_2}^2\rangle - \langle\varepsilon_L\rangle^2]^{1/2}$ in%
35-2	$4x10^{-4}$	0.53	3.0	4.328±.001	0.72-0.99	2775	230	0.21
35-3	$4x10^{-4}$	0.67	4.0	4.318±.002	0.62-0.65	2550	160	0.24
35-4	$4x10^{-4}$	1.00	6.0	4.306±.001	.54-.56	2070	200	0.32
	$4x10^{-4}$	---	8.0	--	Ti + TiC	--	--	--
	$4x10^{-4}$	---	9.7	--	Ti + TiC	--	--	--

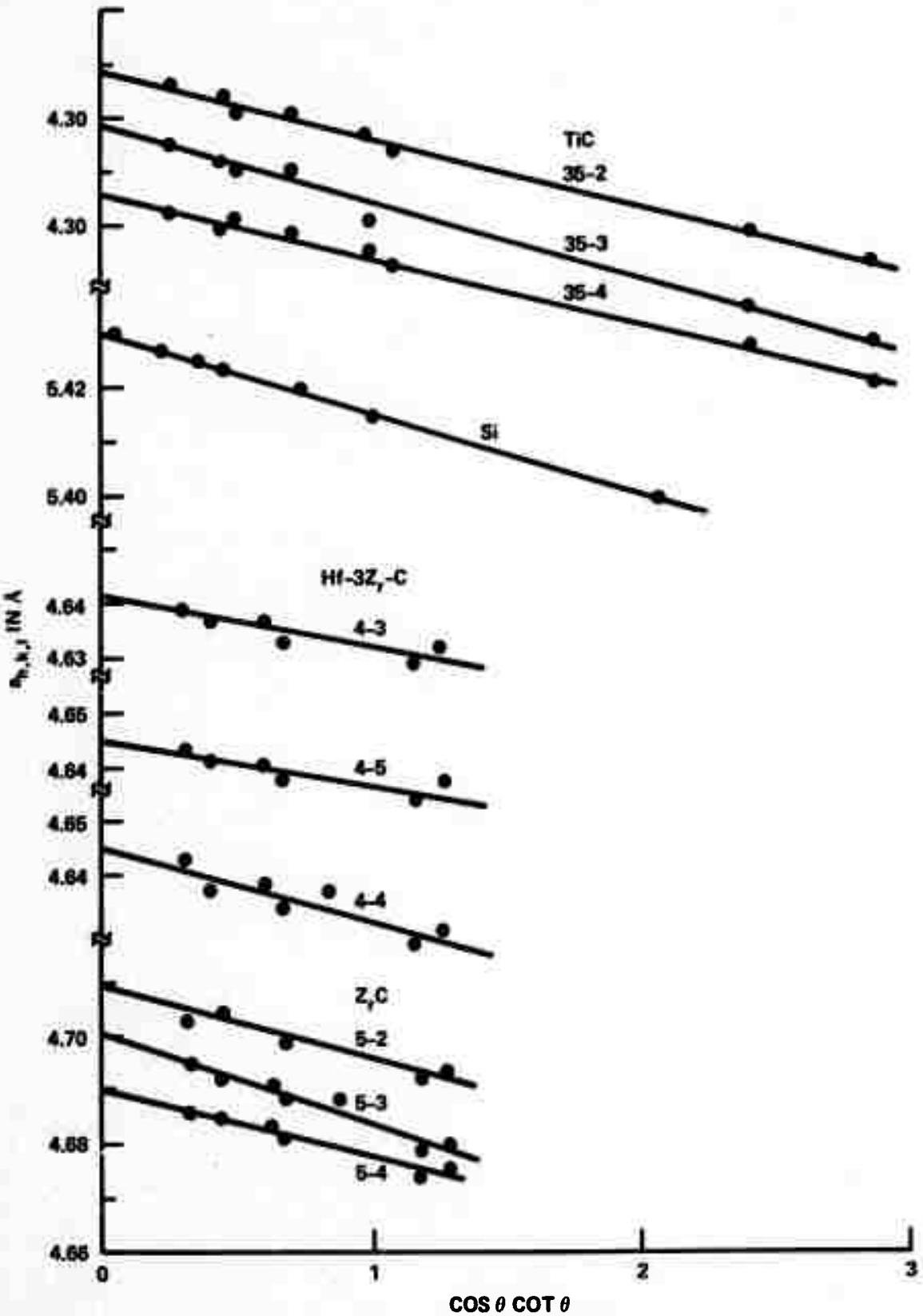

Figure 4. Lattice Parameter $a_{h,k,l}$ as a Function of Cos θ Cot θ

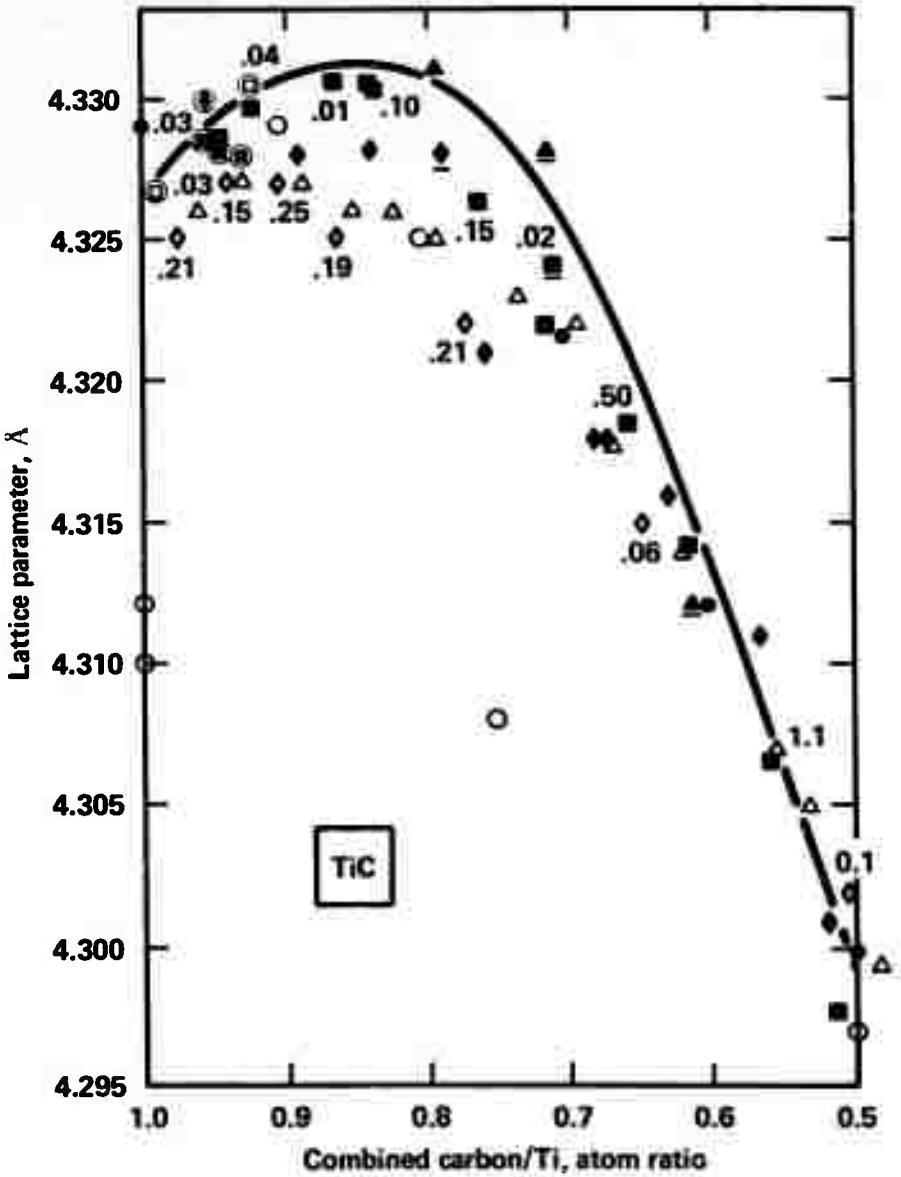

- ◊ Rassaerts et al. (1966)
- ● Costa and Conte (1964) (apparently nominal composition)
- △ Bittner and Goretzki (1962)
- ■ Norton and Lewis (1963)
- ▲ Cadoff, Nielsen, and Miller (1955)
- ♦ Rudy and co-workers (1965a)
- □ Storms (1966)
- ○ Ehrlich (1949)

Melted samples underlined
Encircled samples contain free carbon
Weight % oxygen shown

Figure 5(a). Lattice Parameter Versus C/M Ratio for TiC (Storms')

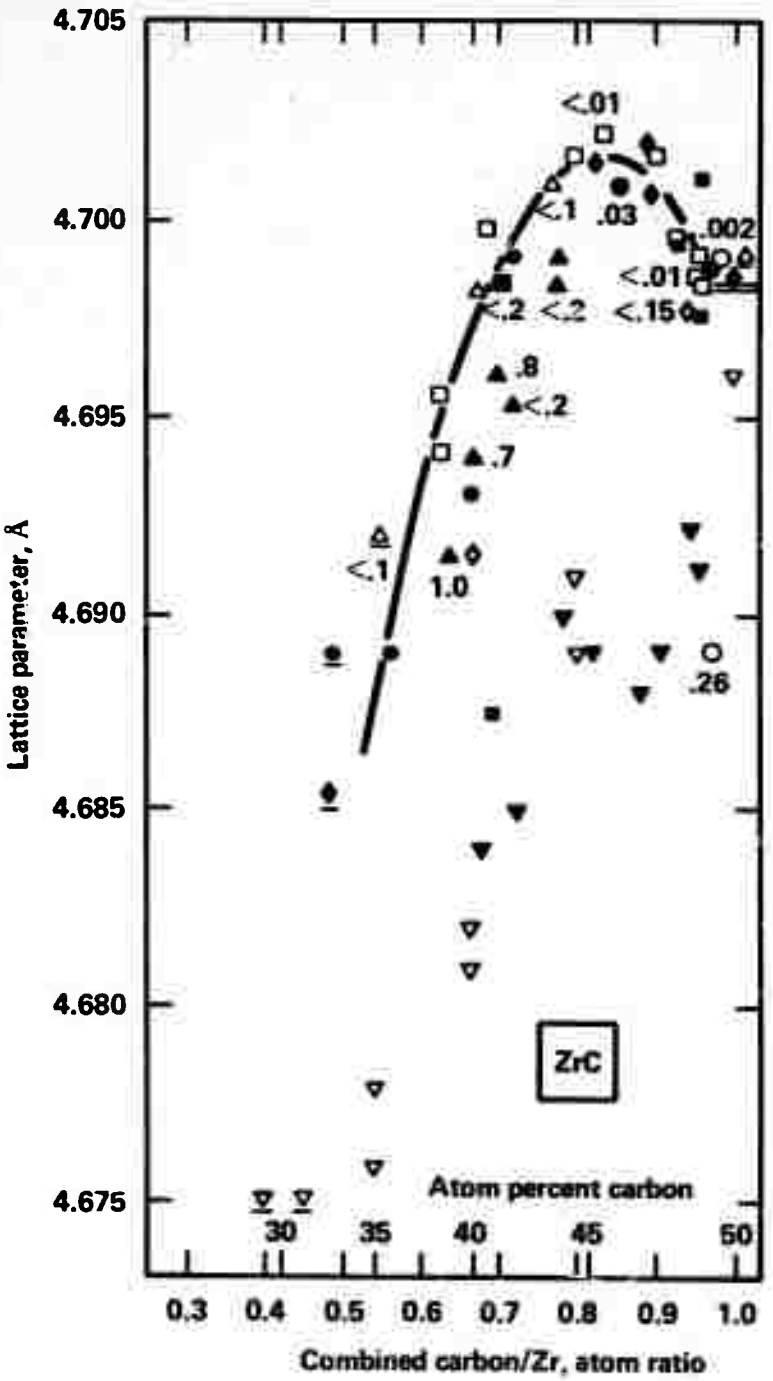

- Sara (1965[a])
- = Average of 5 samples containing free carbon
- ■ Zone refined boule
- ■ Norton and Lewis (1963)
- ◆ Rudy et al. (1965[a])
- ● Storms (1965)
- ◇ Kempter and Fries (1960)
- ○ Grossman (1965)
- ● Wallace et al. (1963)
- ▼ Bittner and Goretzki (1962)
- ▽ Benesovsky and Rudy (1960)
- ▲ Zhelankin et al. (1958)
- △ Henney and Jones (1964) [Arc-melted samples shown]

Two-phase samples underlined. Wt % Oxygen shown.

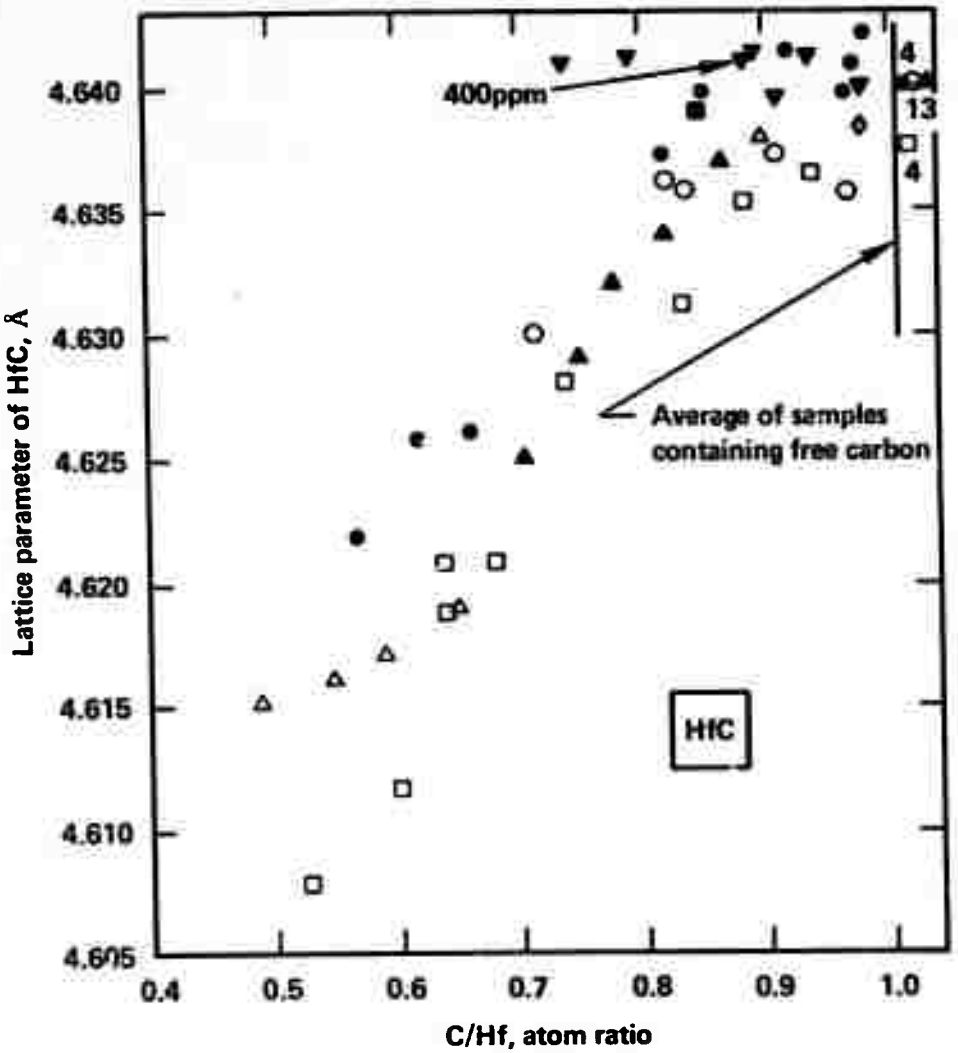

Effect of 4.0 at % Zr

		At % Zr	Anneal
●	Sara & Lowell (1964)	3.1	3150°C
○	Adams & Beall (1963)	3.9	melted
□	Rudy (1965)	4.0	2260,9600°
△	Bittner & Goretzki (1962)	?	2200°
■	Krikorian et al. (1963)	3.5	
▲	Krikorian et al. (1963)	0.04	
◇	Levinson (1964c)	0.08	
▽	Deadmore (1964)	0.02	
▼	Norton & Lewis (1964)	?	2200° open crucible

Figure 5(c). Lattice Parameter Versus C/M Ratio for HfC (Stroms')

There is a considerable scatter in the data from various investigators; for TiC and ZrC, Storms[1] has indicated his best estimate as a solid line. Since the lattice parameter curve is quite flat as C/M approaches unity, the range of C/M values read from the plot for a given lattice parameter becomes larger as the lattice parameter increases i.e., C/M approaches unity. As it was impossible to separate the carbide deposits from the substrate, no direct chemical analysis for carbon content could be carried out.

Since compound synthesis and deposit growth are separate steps in this technique, the stoichiometry of the deposit can be changed by varying the relative amounts of metal vapor and reactive gas. This is illustrated in Tables II and III. With a fixed supply of metal atoms, increase in partial pressure of reactive gas changes the deposit from a mixture of Ti + TiC to TiC of increasing [C/M] ratio, as shown in Table II. Similarly, at a constant partial pressure of C_2H_2, increasing the supply of metal atoms decreases the stoichiometry and ultimately leads to a mixture of Ti + TiC as shown in Table III. This verifies the Reaction Kinetics model for the ARE process proposed earlier. The ability to change stoichiometry is a very desirable feature, since many properties are strongly influenced by the stoichiometry as illustrated by the increase in microhardness with [C/M] ratio, see Tables II and III.

The lattice parameter values of TiC determined in this investigation are in agreement with the values reported in the literature and shown in Fig. 5. The precision of the determination of a_o is lower for the carbide than that of the Si standard, where all a_{hkl} values fall on a straight line when plotted as a function of $\cos\theta \cot\theta$. The scatter of the a_{hkl} values about the straight line in the case of the carbide deposits could

be a consequence of residual stresses σ and stacking faults. In general, the lattice parameter a_{hkl}, as determined from the position of the (hkl) reflection is given by:[10]

$$a_{hkl} = a_o + G_{hkl}\, a_o \alpha + (S_1)_{hkl}\, a_o\, \sigma + m \cos\theta \cot\theta \quad , \tag{5}$$

where α is the stacking fault probability, σ is the residual stress, G_{hkl} and $(S_1)_{hkl}$ are constants[10] which depend upon the crystallographic orientation of the reflecting plane (hkl), and m is in the slope of the straight line.

As shown below the stacking fault probability α is very small in the deposits; thus its effect on the lattice parameter can be neglected Attempts have been made to calculate values of the elastic constant $(S_1)_{hkl}$ according to the procedure outlined in ref. 10, using single crystal elastic moduli.[11] Since the deviation from elastic isotropy is very small for TiC, the values of $(S_1)_{hkl}$ do not show a large scatter about an average elastic constant, and, consequently, the residual stress σ must be very large (>1000 kg/mm^2) to account for the experimental scatter of a_{hkl}; this seems to be an unreasonably large value for the residual stress.

Evidence has been found by Lewis and Billingham[12] for long range order of the vacancy distribution in sub-stoichiometric transition metal carbides. The carbon atoms and metal atoms form alternating close-packed layers in the B1 structure. However, only in every other carbon layer are the octahedral sites completely filled with carbon atoms. The introduction of vacancies on alternating carbon layers will introduce a slight rhombohedral distortion of the lattice. This might produce the scatter of the a_{hkl} values about the straight line when plotted as a function of cosθ cotθ, because some interplaner spacings a_{hkl} will contract more than others.

The particle sizes <D> and strains $[\langle\varepsilon^2_{100}\rangle - \langle\varepsilon\rangle^2_{100}]^{1/2}_{111}$ for L = 100A are also given in Tables II and III. The particle sizes <D> are rather small (about 200A) and isotropic, i.e., within the precision of $\pm$ 10A of the measurement of <D>, the same values were determined in the [111] and [100] directions. This result indicates that the density of stacking faults or growth faults on (111) planes[8] must be very low. The small, coherently diffracting domains are produced by dislocations or dislocation networks in the deposits.

The strains in the TiC deposits are anisotropic, i.e., $\varepsilon_{111}/\varepsilon_{100} = 1.3$ which is a consequence of the anisotropy of the elastic constants and are produced by the strain fields of dislocations.

The microhardness values obtained here agree very well with those reported by Williams and Lye[13] for different [C/M] ratios.

B. Zirconium Carbide

Table IV gives the variation of lattice parameters a_o, the C/M ratio and microhardness of ZrC as a function of synthesis variables. The stoichiometry changes with supply of either reactant as expected. The microhardness values increase with increasing lattice parameter and C/M ratio as expected. The lattice parameter for the hardest samples, Nos. 5-2 and 5-4 are higher than those reported in the literature. As C/M ratio approaches unity, O_2 can substitute the carbon and decrease the lattice parameter, which may account for the maximum in the curves shown in Fig. 5.[1] Our specimens prepared in a vacuum environment may be expected to have a much lower O_2 contamination than the ones reported in the literature which are prepared by reduction reactions followed by pressing and sintering. This would account for the higher lattice parameter since the lattice parameter would continue to increase with C/M ratio. The hardness

Table IV

Variation of Lattice Parameter, $[\frac{C}{M}]$ Ratio and Microhardness with Rate of Deposition and Pressure of Reactive Gas for ZrC

le No.	Rate of Deposition m/min.	$P_{C_2H_2}$ Torr	Lattice Parameter A°	Carbon to Metal Ratio $[\frac{C}{M}]$	Microhardness Kg/mm^2 Load 50 g Knoop Indentor
	2.0	$4x10^{-4}$	4.709±0.002	>0.8*	2800
	5.7	$4x10^{-4}$	4.700±0.002	.69-0.83	2525
	7.6	$4x10^{-4}$	4.690±0.002	.55-.59	2040
	2.3	$3x10^{-4}$	4.705±0.002	>0.8*	2670

possible to estimate since lattice parameter values are higher than those orted in literature (see Fig. 5).

increase is a step with the C/M ratio as would be expected. The highest reported hardness value in the literature[1] is in the range 2600-2800 kg/mm^2 which is in good agreement with the values reported here.

C. (Hf-3Zr) Carbide

Table V gives the variation of lattice parameter, C/M ratio and microhardness as a function of synthesis variables. The precision in lattice parameter determinations is somewhat worse than for TiC and ZrC probably due to residual stresses. Because of the extreme scatter in the data shown in Fig. 4, it is not possible to estimate the C/M ratio. However, the lattice parameter and microhardness values vary with the supply of either reactant in the direction expected as may be seen by comparing specimens 3-3, 3-4, 3-5 and 3-6 in Table V.

The diffraction pattern of only one Hf-3Zr carbide, i.e., the sample exhibiting a microhardness of 2705 Kg/mm^2, was subjected to a Fourier analysis. It was found that the particle size is isotropic and its value is 205A $\pm$ 10A. The strains $[\langle\varepsilon_L^2\rangle - \langle\varepsilon_L\rangle^2]^{1/2}$ decrease with increasing L which represents the distance normal to the reflecting planes. The values at L = 100A were 0.31% in the [111] direction and 0.17% in the [100] direction.

V. Summary and Conclusions

Thick deposits of TiC, ZrC and (Hf-3Zr)C have been prepared at high deposition rates using the ARE process. The stoichiometry of the carbide can be controlled by varying the supply of either reactant. The lattice parameter, C/M ratio and microhardness increased with increasing supply of the carbon containing gas, or decreasing supply of metal vapor. The values of lattice parameter and microhardness agree fairly well with the data reported in the literature. TiC has a very fine grain size

Table V

Variation of Lattice Parameter, $[\frac{C}{M}]$ Ratio and Microhardness with Rate of Deposition and Pressure of Reactive Gas for (Hf-3Zr)C

Sample No.	Rate of Deposition m/min.	$P_{C_2H_2}$ Torr	Lattice Parameter A°	Microhardness Kg/mm^2 Load 50 g Knoop Indentor
4-2	2.6	$4x10^{-4}$	4.644±0.001	3035
4-3	3.5	$4x10^{-4}$	4.642±0.002	2705
4-4	3.8	$4x10^{-4}$	4.645±0.002	2445
4-5	4.0	$4x10^{-4}$	4.645±0.003	2330
3-3	3.8	$1.5x10^{-4}$	4.605±0.003	1890
3-4	3.8	$3.3x10^{-4}$	4.644±0.003	2210
3-5	3.8	$5x10^{-4}$	4.645±0.002	2630
3-6	3.8	$7-8x10^{-4}$	4.645±0.001	3840

(<1000A) with a subgrain size of 200A and exhibits a very strong bond with the substrate.

It would appear that this is a powerful technique for the rapid and economical deposition of hard adherent layers on soft substrates and should find industrial uses.

References

1. Edmund K. Storms, The Refractory Carbides, Academic Press, N.Y., 1967.

2. R.F. Bunshah, Patent Application, University of California.

3. R.F. Bunshah and A.C. Raghuram - Activated Reactive Evaporation - to be published in Journal of Vac. Sci. and Tech., November-December 1972.

4. L. Holland - "Vacuum Deposition of Thin Films," Chapman and Hall, London, 1966.

5. B.B. Kosicki and D. Khang, Journal of Vac. Sci. and Tech., 6, 592, (1969).

6. R.F. Bunshah and R.S. Juntz - to be published in Trans. Met. Soc. AIME, 1972

7. R.F. Bunshah and R.T. Webster - Journal of Vac. Sci. and Tech., 8, VM95 (1971)

8. C.N.J. Wagner and E.N. Aqua, Advances X-Ray Anal. 1, 46, (1964).

9. A.C. Raghuram and R.F. Bunshah, "The effect of Substrate Temperature on the Structure of TiC Deposited by Activated Reactive Evaporation," to be published in Journal of Vac. Sci. and Tech., Nov/Dec. 1972.

10. C.N.J. Wagner, J.P. Boisreau and E. Aqua, Trans. Met. Soc. AIME, 233, 1280 (1965).

11. J.J. Gilman and B.W. Roberts, J. App. Phys. 32, 1405 (1961).

12. M.H. Lewis and J. Billingham, JEOL News 10, #1, 8 (1972).

13. W.S. Williams and R.G. Lye, Technical Documentary Report ML-TDR-64-25, Part II, March 1965, pg. 23. Issued by Air Force Materials Laboratory, Wright-Patterson AFB, Ohio

Acknowledgements

The Zr sheet used as a substrate and evaporant rods of Zr and Hf-3Zr were very kindly supplied by Teledyne Wah Chang Corporation through the courtesy of Mr. R. T. Webster. The authors are also very grateful to Dr. L. Wegmann of Balzers High Vacuum Corporation for the photomicrographs of the deposits using their photo-emission electron microscope. This work was performed under ARPA Grant DAHC 15 70 G 15.